Electronic Supplementary Information

A through-space charge transfer pyrene-based fluorophore with anti-quenching behavior for deep-blue organic light-emitting devices

Ru-Jia Wang,[a,b] Fan Zheng[a,b], Xiao-Long Liu[a,b], Yu-Lan Wu[a,b], Jia-Ming Jin,[a,b], Ze-Yan Li [a,b], Wen-Cheng Chen[a,b]*, Yanping Huo[a,b,c]*

[a]School of Chemical Engineering and Light Industry, Guangdong University of Technology, Guangzhou, P. R. China

[b]Guangdong Provincial Laboratory of Chemistry and Fine Chemical Engineering Jieyang Center, Jieyang, P. R. China

[c]Analytical & Testing Center, Guangdong University of Technology, Guangzhou, P. R. China

E-mail: wencchen@gdut.edu.cn (W.-C. Chen); yphuo@gdut.edu.cn (Y. Huo)

General information

^{1}H and ^{13}C NMR spectra were obtained on a Bruker AVANCE III HD-400 NMR spectrometer. Mass analyses were performed on a Thermo Scientific Q Exactive instrument. Decomposition and glass transition temperatures were measured respectively on a STA409PC Thermogravimetric Analyzer and a NETZSCH thermal analyzer (DSC 204 F1) at a heating rate of 10 °C min^{-1} under a nitrogen atmosphere. UV-vis absorption spectra were recorded using a Shimadzu UV-2700 spectrophotometer. Photoluminescence (PL) spectra, lifetimes, and PL quantum yield (PLQY) were measured on an Edinburgh FLS980 spectrometer. Single crystal X-ray diffraction measurements were performed on a Rigaku Oxford Diffraction SuperNova dual source diffractometer. Cyclic voltammetry (CV) was carried out in acetonitrile with tetra-*n*-butylammonium hexafluorophosphate (Bu_4NPF_6) (0.1 M) at a scan rate of 100 mV s^{-1} using an Autolab PGSTAT302N electrochemical workstation with a three-electrode cell (Ag/AgCl standard electrode as the reference electrode, Pt wire counter electrode, and glassy carbon working electrode). Ferrocene was used as internal standard with an absolute highest occupied molecular orbital (HOMO) level of -4.80 eV. The energy levels of the HOMO and lowest unoccupied molecular orbital (LUMO) were estimated using the equations [HOMO = -(E_{ox} + 4.8) eV] and [LUMO = (HOMO + E_g) eV], respectively, where E_{ox} represents the onset oxidation potential, and E_g is the optical energy gap derived from the absorption onset.

Device fabrication and measurement

Devices were fabricated on indium tin oxide (ITO) coated glass substrates with a sheet resistance of 15 Ω sq^{-1}. Before use, the ITO substrates were swabbed with Decon-90 solution, and treated by 10-min ultrasonic baths in deionized water, and then rinsed with isopropanol. The solvent on the surface was removed with dry N_2 flow, and then the substrates were further dried in an oven at 120 °C for at least 2 h. After 15 min UV-ozone treatment, the substrates were loaded into a deposition chamber with a vacuum better than 10^{-6} Torr. Current density-voltage characteristics and electroluminescence spectrum were recorded with a

Keithley 2400 power source and a Spectrascan PR745 photometer, respectively. Device measurement was performed under ambient conditions without encapsulation.

Theoretical Calculations

The molecular structure was optimized using the Gaussian 09 program employing density functional theory (DFT) at the B3LYP/6-31G(d) level in the ground state. Subsequently, utilizing the optimized ground-state geometry, the highest occupied molecular orbital (HOMO) and lowest unoccupied molecular orbital (LUMO) levels were estimated. Additionally, the energy levels of excited states were determined by employing the time-dependent DFT (TD-DFT) method at the m062x/6-31g(d,p) level. Hirshfeld surface based on the single crystal structure of PySAF (CCDC no. 2361680) was performed using Multiwfn 3.8[1] and visualized with the VMD program.

Synthesis

The reagents and solvents utilized for synthesis and measurements were used as received from suppliers without additional purification. 10-phenyl-10*H*-spiro[acridine-9,9'-fluorene] (SAF) was prepared according to the reported procedures.[2]

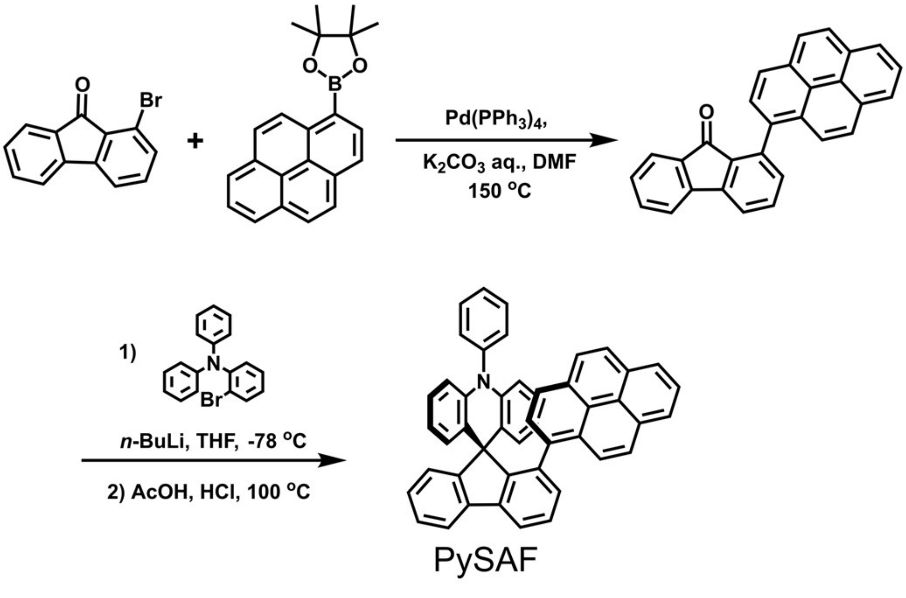

Scheme S1 Synthesis of PySAF.

1-(pyren-1-yl)-9*H*-fluoren-9-one: Under a nitrogen atmosphere, 1-bromo-9*H*-fluoren-9-one (1.0 g, 3.86mmol), 4,4,5,5-tetramethyl-2-(pyren-1-yl)-1,3,2-dioxaborolane (1.5 g, 4.57 mmol), $Pd(PPh_3)_4$ (360mg, 311.5 μmol), K_2CO_3 aq. (2 mL, 2 mol L^{-1}) and DMF (15 mL) were added to a three-necked flask. The reaction mixture was stirred at 150 °C for 24 h. After cooling to room temperature, the mixture was poured into water and extracted with CH_2Cl_2 (3 × 20 mL). The combined organic extracts were dried over anhydrous $MgSO_4$, filtered, and the solvent was evaporated. The crude product was purified by silica gel column chromatography using petroleum ether/dichloromethane (1:8, v:v) as eluent. 1-(pyren-1-yl)-9*H*-fluoren-9-one was obtained as a yellow solid in 85% yield. ^{1}H NMR (400 MHz, DMSO-d_6) δ 8.34 (d, J = 8.4 Hz, 2H), 8.26 (d, J = 6.7 Hz, 3H), 8.12 – 8.03 (m, 2H), 8.02 – 7.94 (m, 2H), 7.92 (d, J = 7.4 Hz, 1H), 7.83 – 7.73 (m, 2H), 7.64 (t, J = 6.8 Hz, 1H), 7.46 – 7.29 (m, 3H). MS (APCI): calcd for $C_{29}H_{16}O$ $[M+H]^+$ 381.45, found 381.05.

10-phenyl-1'-(pyren-1-yl)-10*H*-spiro[acridine-9,9'-fluorene] (PySAF): 2-bromotriphenylamine (5.45 g, 16.81 mmol) was dissolved in 40 mL dry THF in a three-necked flask under N_2, and then the mixture was cooled to -78 °C under stirring. 6.5 mL *n*-butyl lithium (16.25 mmol) was added dropwise using a syringe. The mixture was allowed to stir for 1 h at the same temperature, followed by adding 100 mL 1-(pyren-1-yl)-9*H*-fluoren-9-one THF solution over 30 min via dropping funnel. The reaction was gradually warmed up to room temperature for further 8 h. 10 mL water was added to quench the reaction and the solvent was removed under reduced pressure. The resulting raw product was dissolved in AcOH (100 mL) and hydrochloric acid (10 mL), and the mixture was stirred at 100 °C overnight. After cooling down, the solvent was evaporated via a rotary evaporator. The product was further purified by column chromatography using petroleum ether/CH_2Cl_2 (1:10, v:v) as eluent to give a white powder (2.90 g, 81.9%). ^{1}H NMR (400 MHz, DMSO-d_6) δ 8.31 – 8.26 (m, 2H), 8.24 – 8.18 (m, 2H), 8.12 (d, J = 7.6 Hz, 1H), 8.06 (d, J = 6.6 Hz, 1H), 7.99 (t, J = 7.6 Hz, 1H), 7.76 (d, J = 7.8 Hz, 1H), 7.63 (t, J = 7.5 Hz, 1H), 7.48 – 7.40 (m, 2H), 7.24 (t, J = 7.4 Hz, 2H), 7.22 – 7.06 (m, 4H), 6.96 (d, J = 9.2 Hz, 1H), 6.88 (ddd, J = 8.5, 7.0, 1.6 Hz, 1H), 6.72 (d, J = 7.8 Hz, 1H), 6.65 – 6.60 (m, 1H), 6.38 – 6.32 (m, 2H), 6.25 – 6.16 (m, 2H), 5.93 (s, 2H), 5.58 (dd, J = 8.4, 1.2 Hz, 1H), 4.71 (dd, J = 8.4, 1.2 Hz, 1H). ^{13}C NMR (101 MHz, Chloroform-*d*) δ 140.34, 139.94, 139.60, 138.72, 135.05, 131.16, 131.13, 130.73, 130.46, 130.25, 130.20, 129.31, 129.05, 128.82, 127.68, 127.60, 127.41, 127.20, 127.13, 126.90, 126.49, 126.44, 126.16, 125.66, 125.36, 124.65, 124.49, 124.46, 123.95, 123.25, 119.70, 119.45, 114.44, 113.82. MS (APCI): calcd for $C_{47}H_{29}N$ $[M+H]^+$ 608.76, found 608.16.

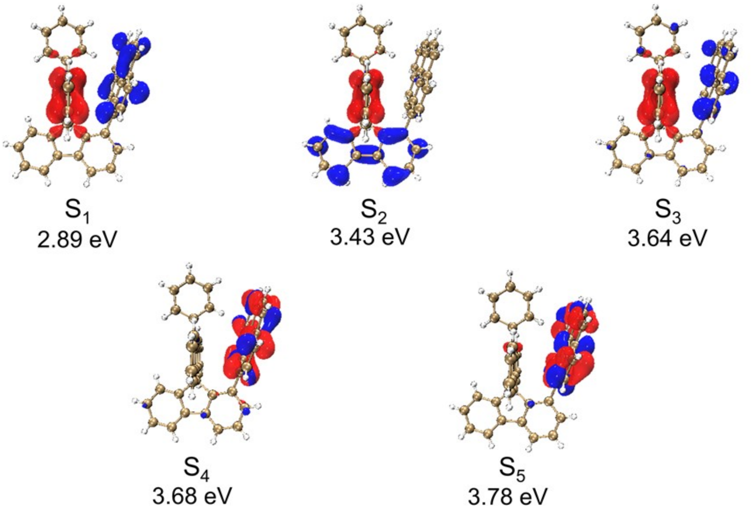

Fig. S1 Natural transition orbital analysis for the singlet excited states of PySAF (red: hole, blue: electron).

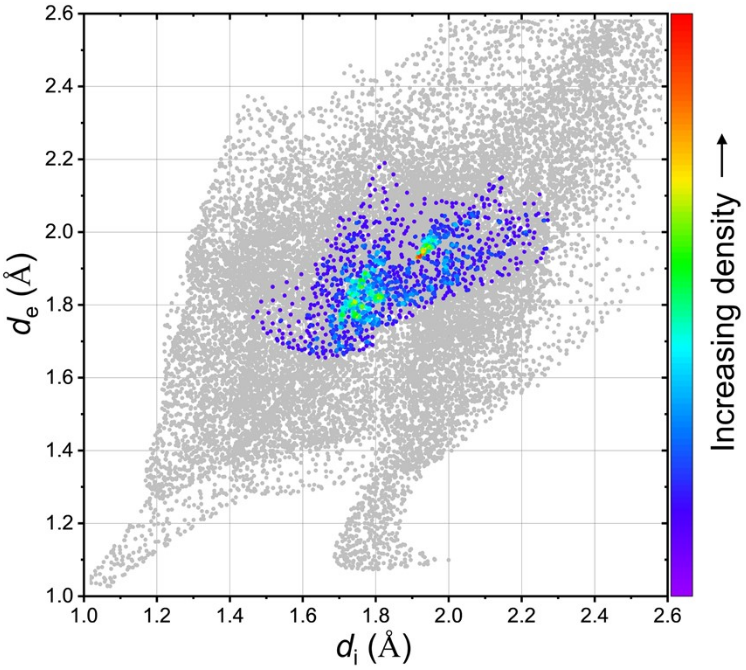

Fig. S2 Hirshfeld decomposed fingerprint plot for the intramolecular C···C contacts on the pyrene plane in PySAF (with the full fingerprint plot indicated in grey). d_i represents the distance from a point on the surface to the nearest nucleus inside the surface, while d_e denotes the distance from a point on the surface to the nearest nucleus outside the surface.

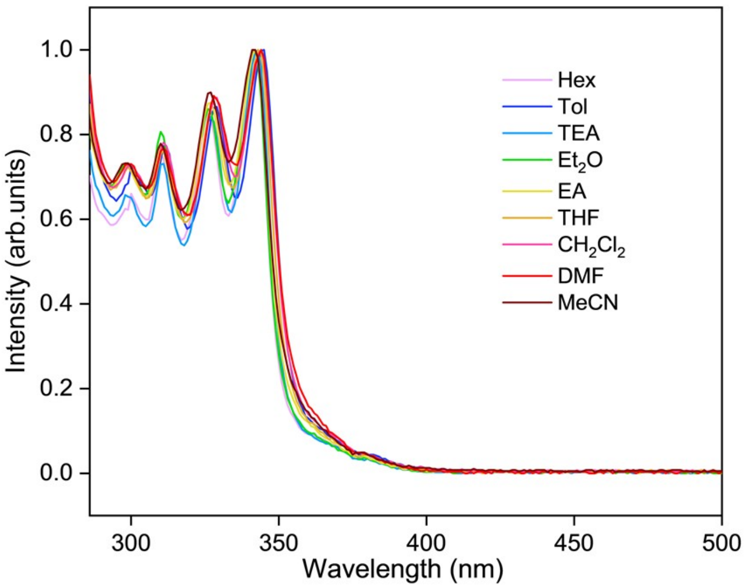

Fig. S3 Absorption spectra of PySAF in different solvents (10^{-5} mol L^{-1}).

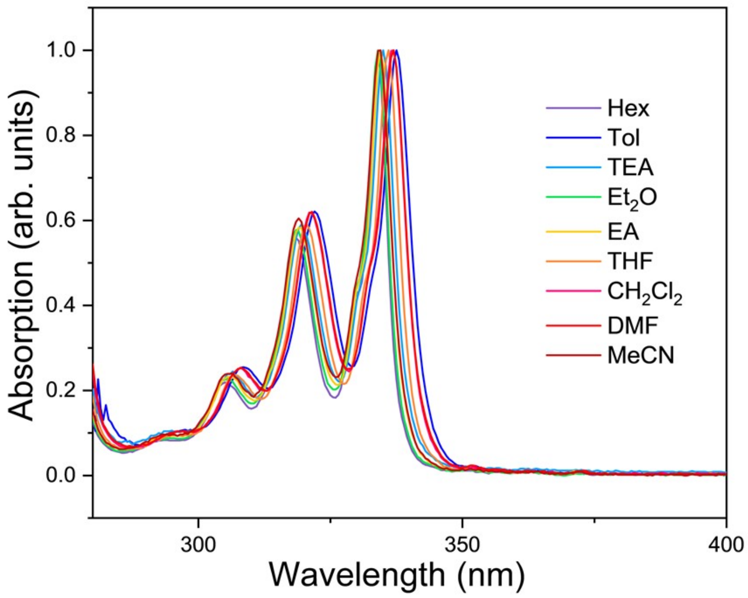

Fig. S4 Absorption spectra of Pyrene in different solvents (10^{-5} mol L^{-1}).

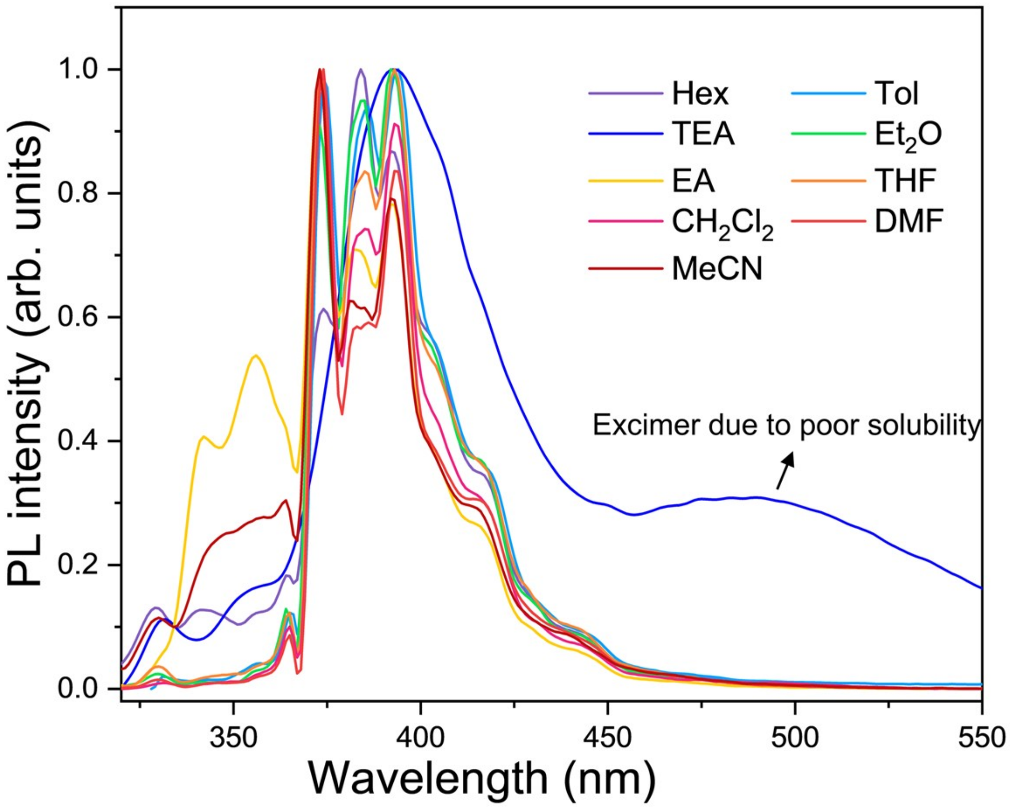

Fig. S5 PL spectra of Pyrene in different solvents (10^{-5} mol L^{-1}).

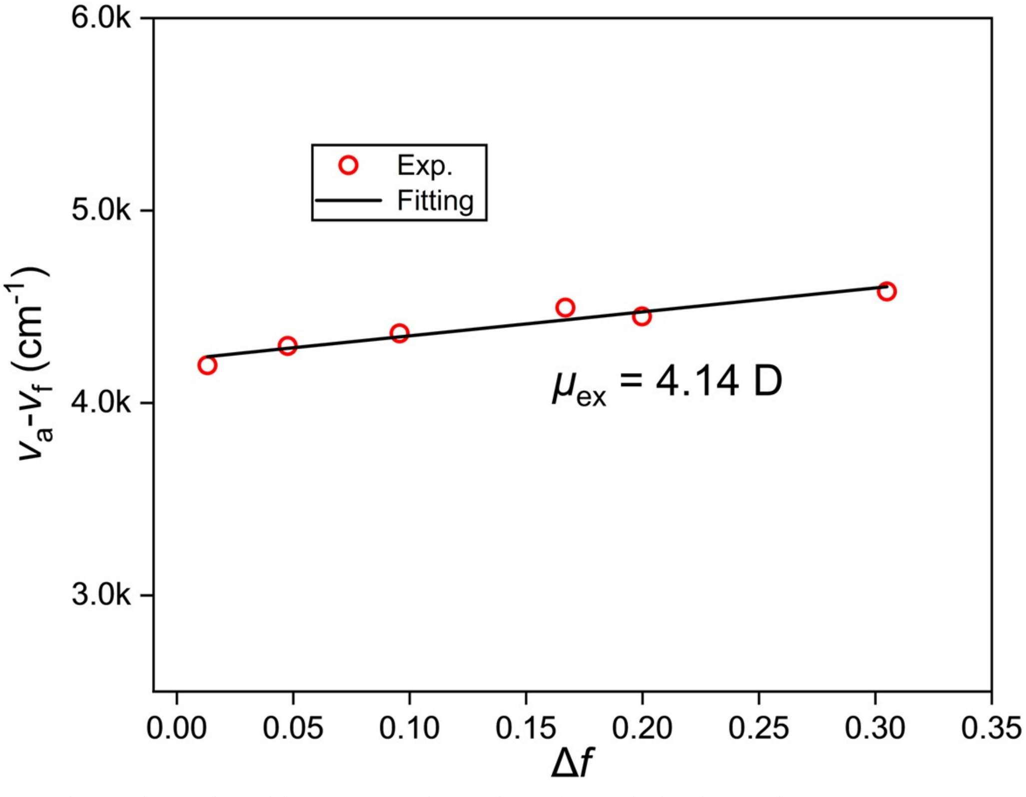

Fig. S6 Plot of the Stokes shift (v_a-v_f) against orientation polarization (Δf) for pyrene.

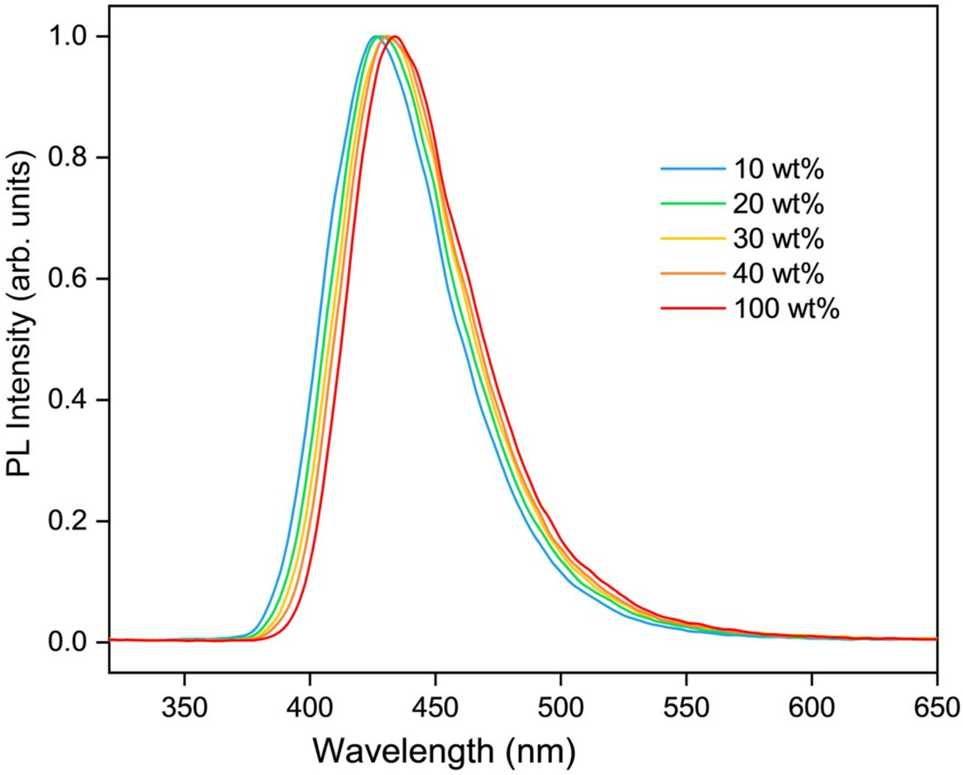

Fig. S7 PL spectra of PySAF's doped films with different doping level (host: mCP).

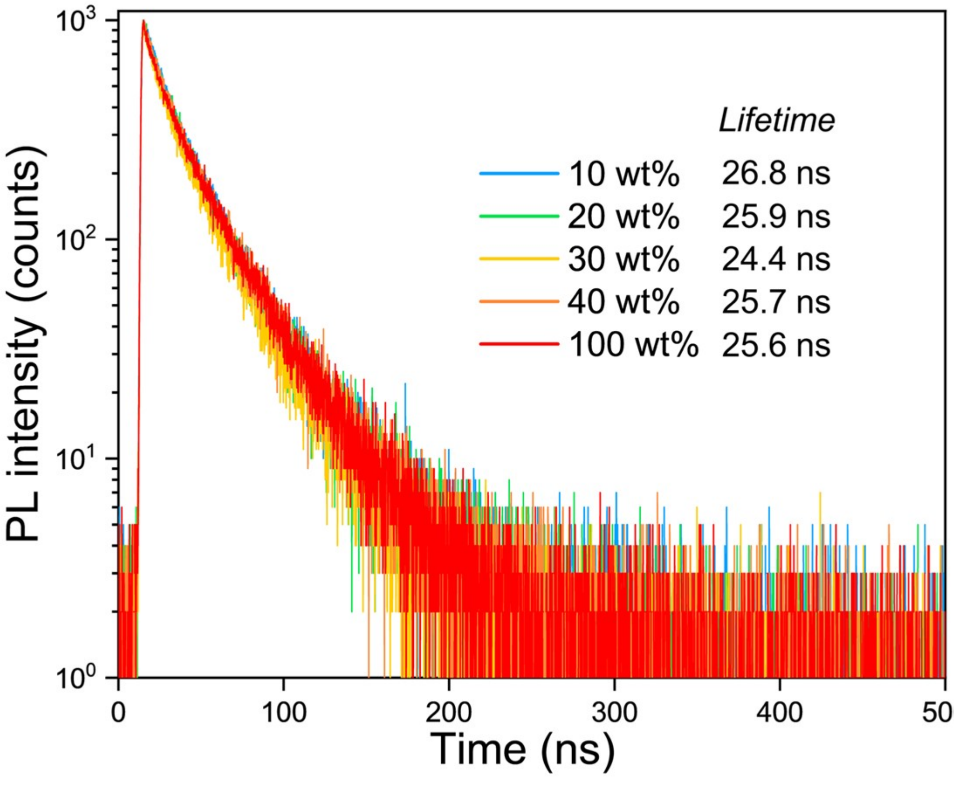

Fig. S8 Transient PL decay curves of PySAF's doped films with different doping level (host: mCP).

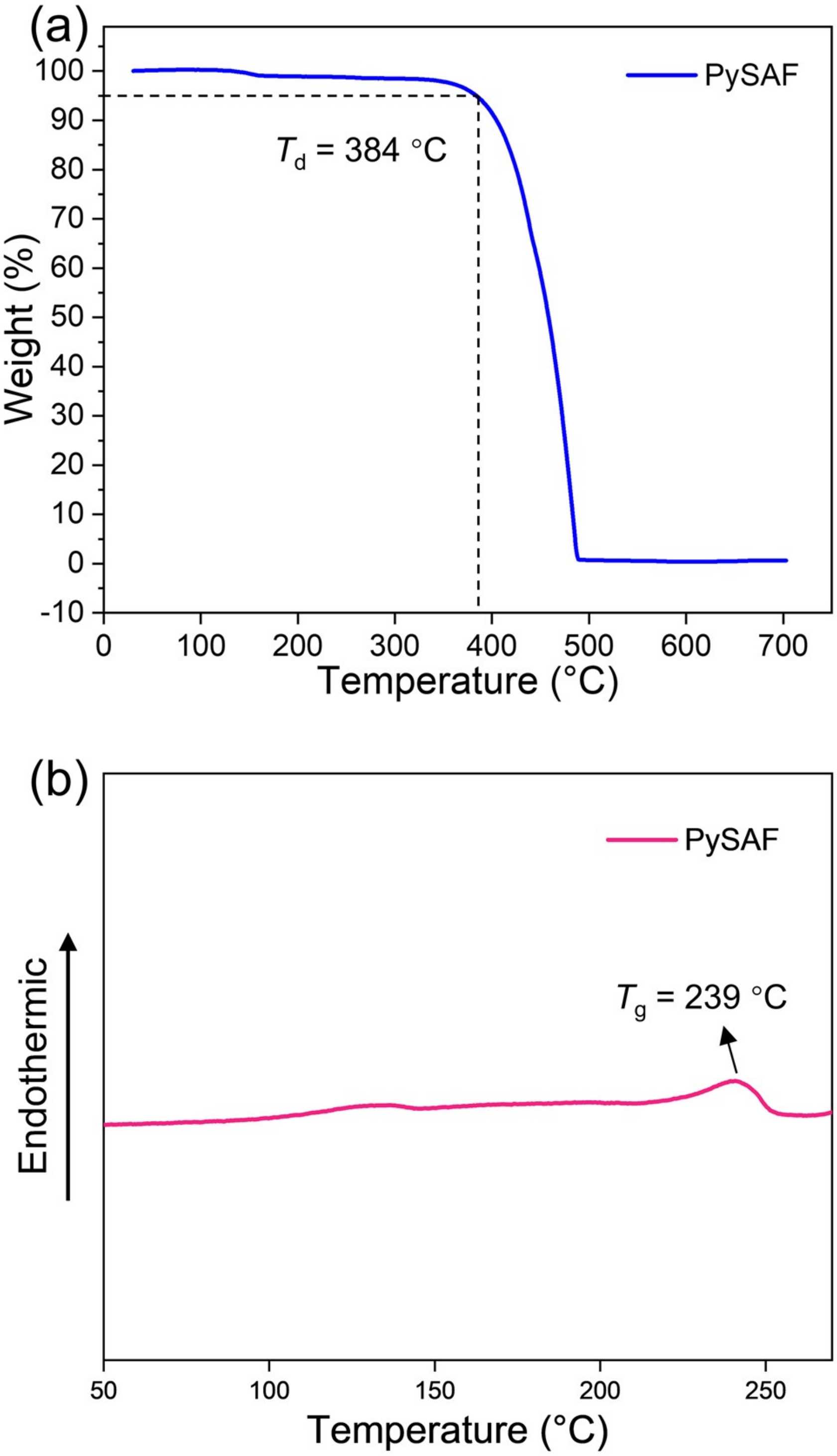

Fig. S9 (a) Thermogravimetric analysis and (b) differential scanning calorimetry measurements for PySAF.

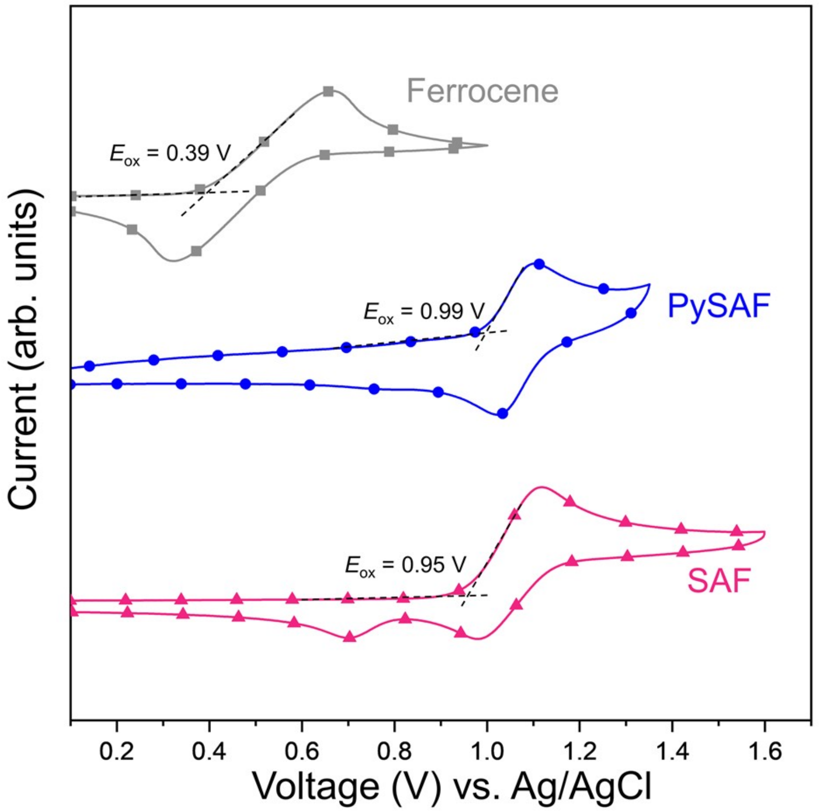

Fig. S10 Cyclic voltammograms for oxidation of ferrocene (as reference), PySAF and SAF.

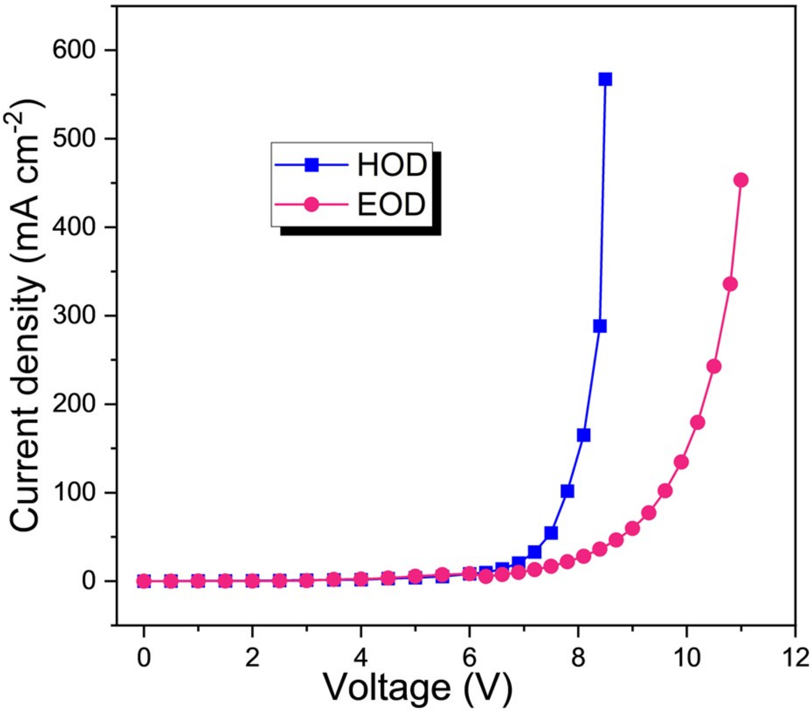

Fig. S11 Current density-voltage characteristics of hole-only devices (HOD) and electron-only device (EOD). The HOD and EOD have configurations of respectively ITO /NPB (10 nm)/PySAF (70 nm)/NPB (10 nm)/Al (100 nm) and ITO/TmPyPB (10 nm)/ PySAF (70 nm)/TmPyPB (10 nm)/LiF (1 nm)/Al (100 nm).

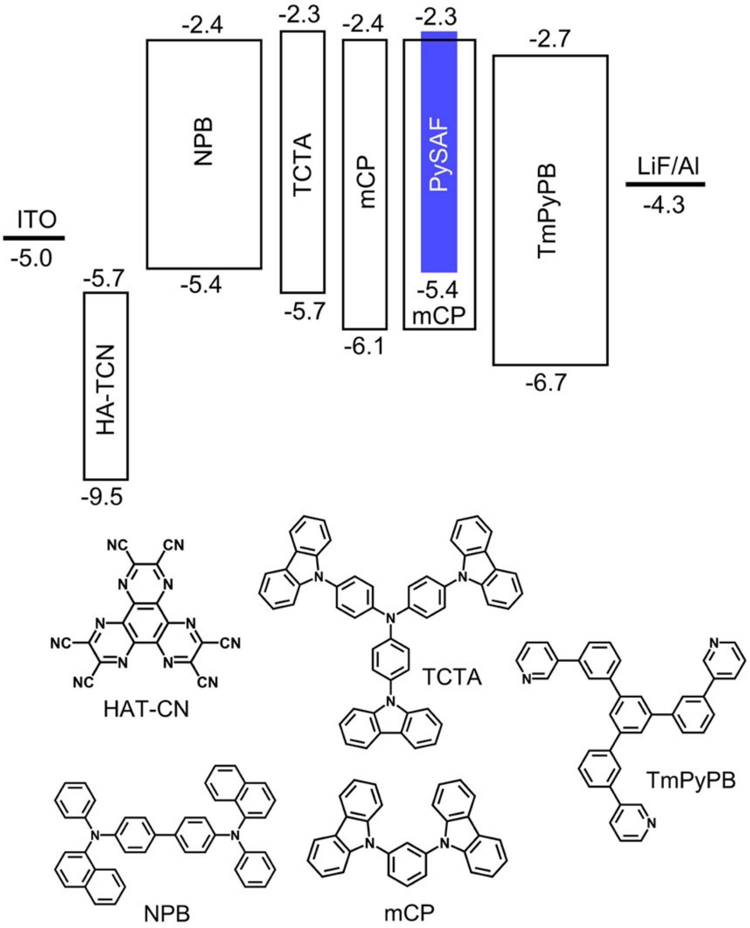

Fig. S12 Energy-level diagram and chemical structures of the materials for device fabrication (device structure: ITO/ HATCN (10 nm)/NPB (50 nm)/TCTA (10 nm)/mCP (5 nm)/mCP: *x* wt% PySAF (20 nm)/TmPyPB (40 nm)/LiF (1 nm)/Al (100 nm) (*x* = 10, 20, 30, 100)).

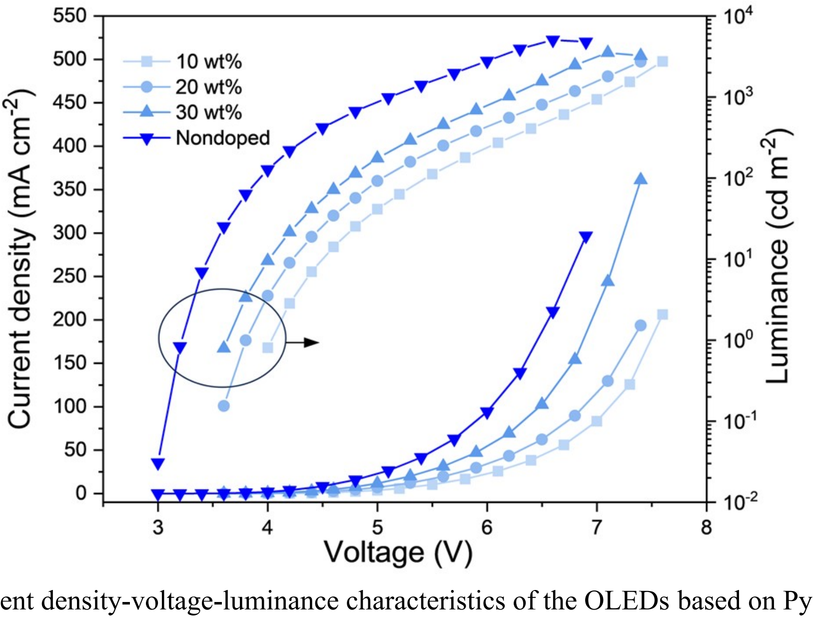

Fig. S13 Current density-voltage-luminance characteristics of the OLEDs based on PySAF.

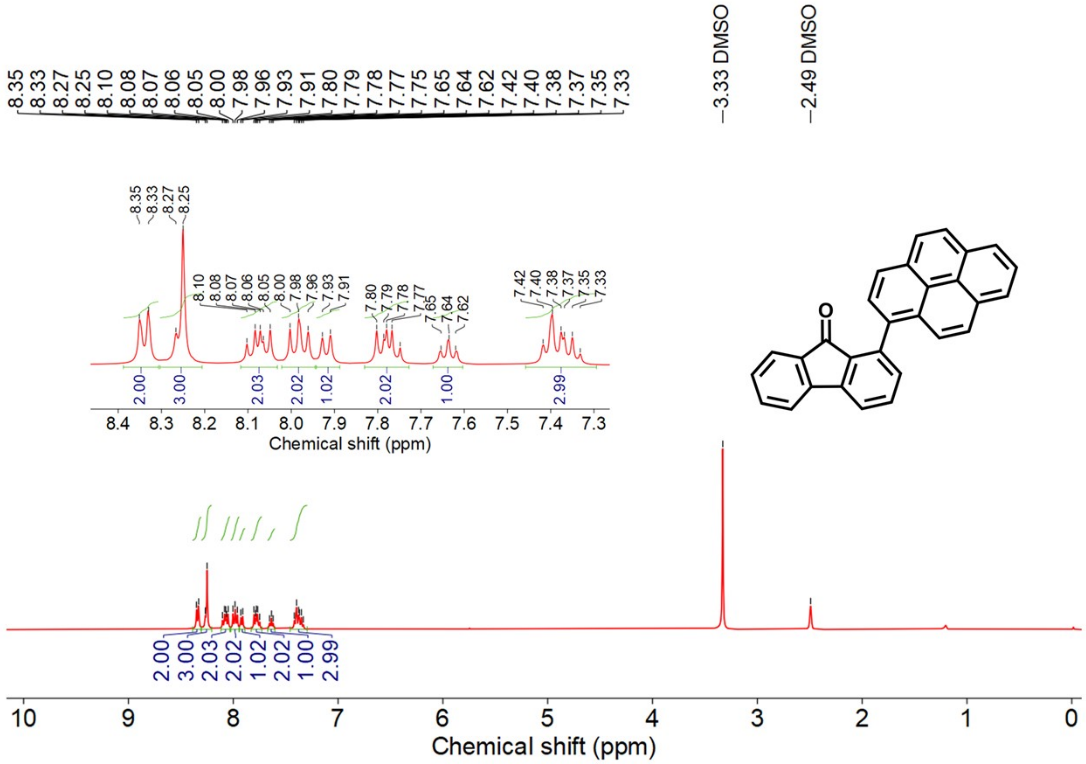

Fig. S14 ^{1}H NMR chart of 1-(pyren-1-yl)-9*H*-fluoren-9-one.

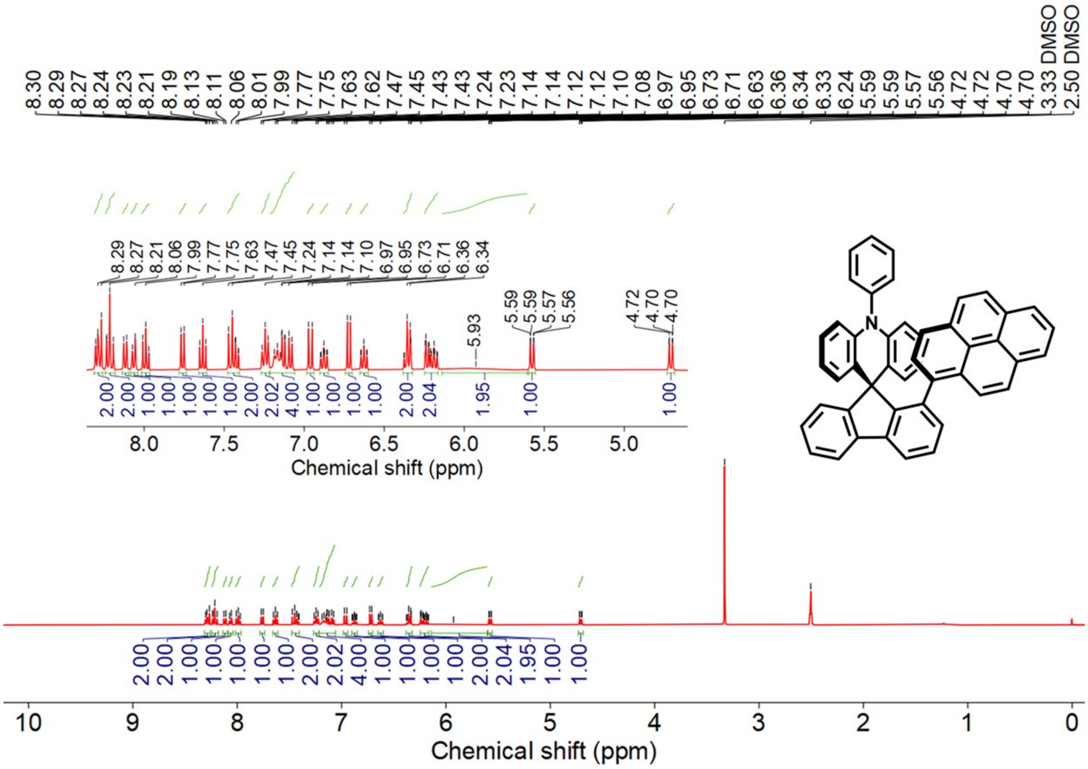

Fig. S15 ^{1}H NMR chart of PySAF.

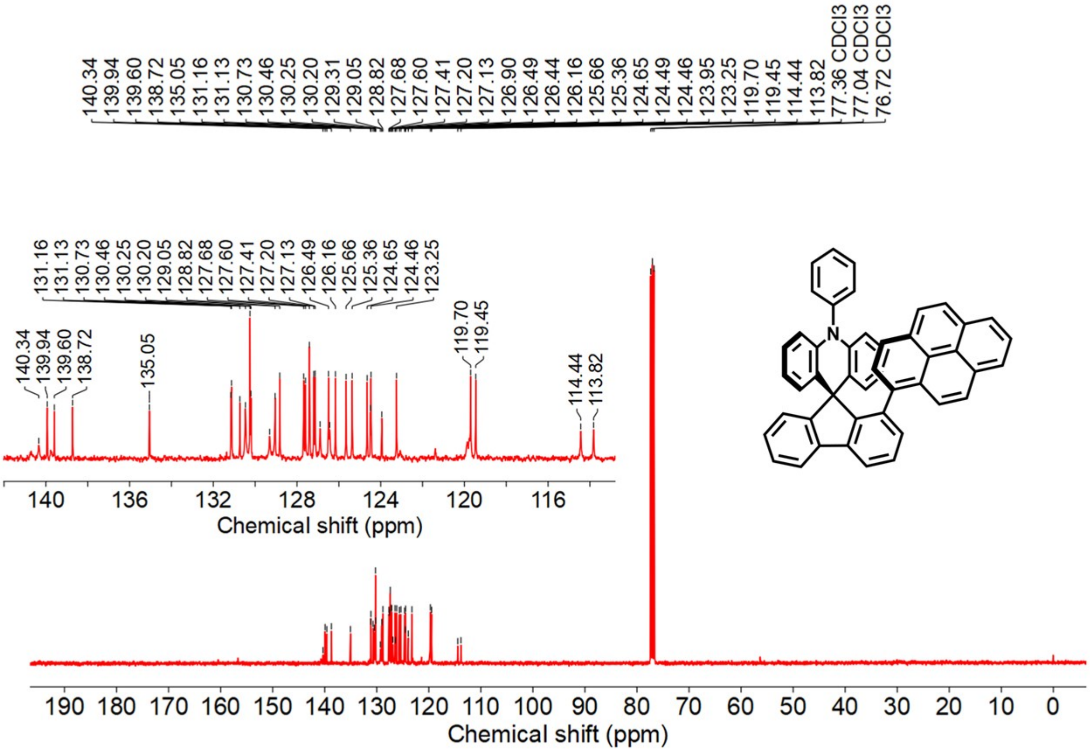

Fig. S16 ^{13}C NMR chart of PySAF.

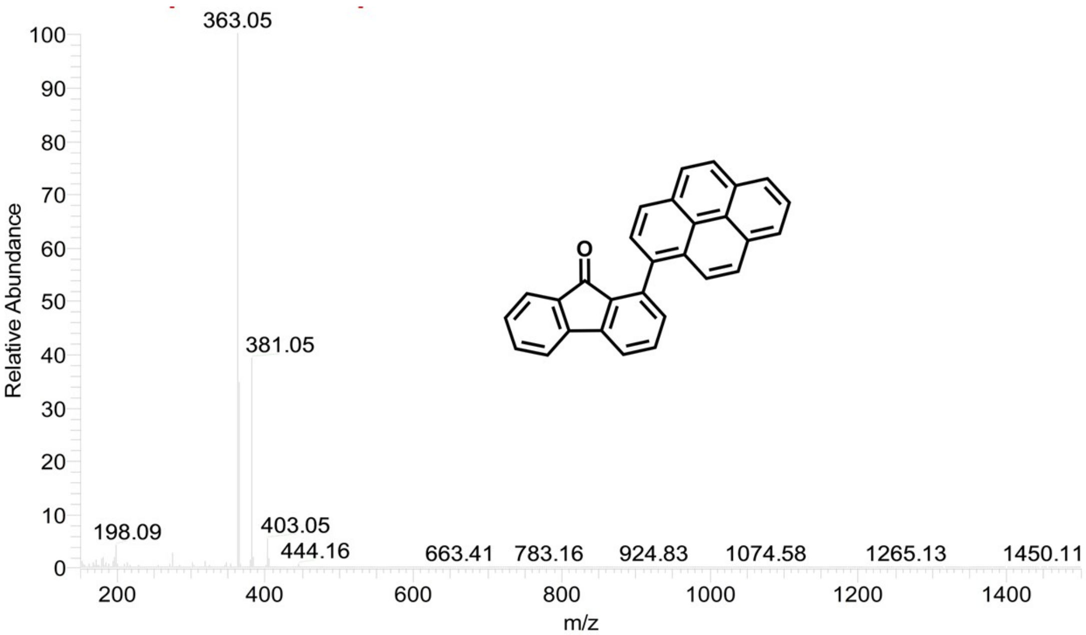

Fig. S17 MS chart of 1-(pyren-1-yl)-9*H*-fluoren-9-one.

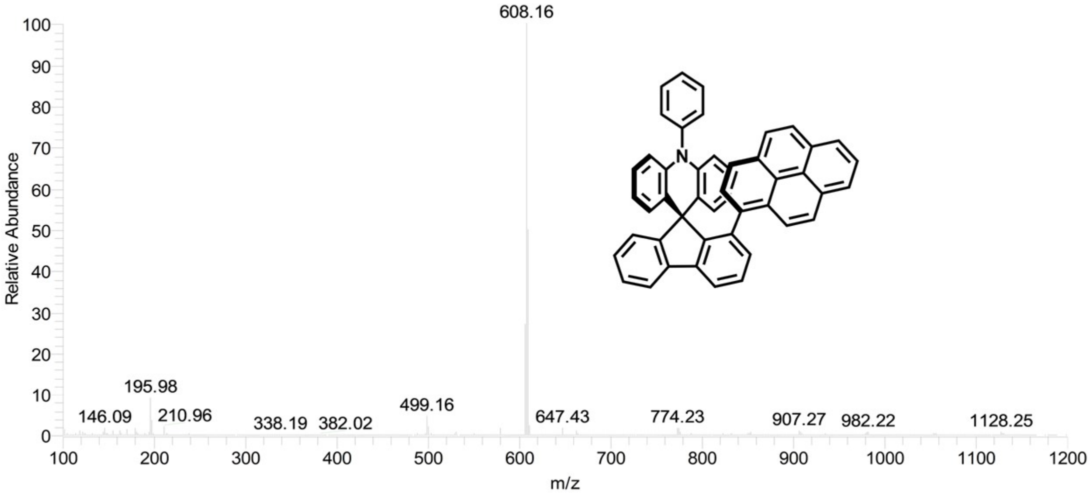

Fig. S18 MS chart of PySAF.

Table S1. Crystallographic data and structure refinement for PySAF.

Compound	PySAF
Empirical formula	$C_{47}H_{29}N•CH_2Cl_2$
CCDC no.	2361680
Formula weight	692.64
Temperature/K	293.15
Crystal system	triclinic
Space group	P-1
a/Å	10.6735(3)
b/Å	11.3393(3)
c/Å	15.9814(5)
α/°	96.998(2)
β/°	104.429(2)
γ/°	106.090(2)
Volume/Å^3	1761.56(9)
Z	2
ρ_{calc}g/cm^3	1.306
μ/mm^{-1}	1.929
F(000)	720.0
Crystal size/mm^3	0.15 × 0.13 × 0.12
Radiation	Cu Kα (λ = 1.54184)
2Θ range for data collection/°	5.834 to 153.594

Index ranges	$-13 \le h \le 9$, $-14 \le k \le 14$, $-20 \le l \le 20$
Reflections collected	21806
Independent reflections	7137 [R_{int} = 0.0276, R_{sigma} = 0.0320]
Data/restraints/parameters	7137/0/461
Goodness-of-fit on F^2	1.080
Final R indexes [I≥2σ (I)]	R_1 = 0.0602, wR_2 = 0.1777
Final R indexes [all data]	R_1 = 0.0718, wR_2 = 0.1896
Largest diff. peak/hole/e Å^{-3}	0.69/-0.63

Table S2. Physical properties of PySAF.

λ_{abs}[a] (nm)	λ_{PL}[b] (nm)	PLQY[c] (%)	T_d[d] (°C)	T_g[e] (°C)	E_{HOMO}[f] (eV)	E_{LUMO}[g] (eV)
345	401	87.6	332	162	-5.47	-2.99

[a]Absorption peak, [b]photoluminescence peak, [c]photoluminescence quantum yield in dilute toluene solution (10^{-5} mol L^{-1}). [d]Decomposition temperature (5% weight loss). [e]Glass transition temperature. [f]Measured by cyclic voltammetry. [g]Calculated by $E_{LUMO} = E_{HOMO} + E_g$.

Table S3. Detailed photophysical data of PySAF in different solvents.

Solvent	ε[a]	n[b]	Δf[c]	λ_a[d] (nm)	λ_f[e] (nm)	ν_a-ν_f[f] (cm^{-1})
n-hexane	1.89	1.3727	0.0008	342	408	4730
Toluene	2.38	1.4969	0.0132	344	430	5814
Triethylamine	2.42	1.401	0.0477	343	423	5514
Butyl ether	3.08	1.399	0.0957	343	426	5680
Diethyl ether	4.33	1.352	0.1669	342	433	6145
Ethyl acetate	6.02	1.372	0.1998	342	455	7262
THF	7.58	1.407	0.2096	343	456	7225
Dichoromethane	8.93	1.424	0.2172	344	466	7611
DMF	36.7	1.431	0.2742	344	485	8451
ACN	36.64	1.344	0.3050	341	486	8749

[a] Dielectric constant. [b]Refractive index. [c]Orientation polarization of solvents, calculated from $\Delta f = (\varepsilon-1)/(2\varepsilon+1)-(n^2-1)/(2n^2+1)$. [d] Absorption and [e]fluorescence emission maximum. [f] Stokes shift.

Table S4. Detailed photophysical data of pyrene in different solvents.

Solvent	ε^a	n^b	Δf^c	$\lambda_a{}^d$ (nm)	$\lambda_f{}^e$ (nm)	ν_a-$\nu_f{}^f$ (cm^{-1})
Toluene	2.38	1.4969	0.0132	337	392.5	4196
Triethylamine	2.42	1.401	0.0477	335.5	392	4296
Butyl ether	3.08	1.399	0.0957	335.5	393	4361
Diethyl ether	4.33	1.352	0.1669	334	393	4495
Ethyl acetate	6.02	1.372	0.1998	334.5	393	4450
ACN	36.64	1.344	0.3050	334.5	395	4579

[a] Dielectric constant. [b]Refractive index. [c]Orientation polarization of solvents, calculated from $\Delta f = (\varepsilon-1)/(2\varepsilon+1)-(n^2-1)/(2n^2+1)$. [d] Absorption and [e]fluorescence emission maximum. [f] Stokes shift.

Table S5. Key parameters of the OLEDs based on PySAF.

Dopant conc. (wt%)	V_{on} (V)	λ_{EL} (nm)	CIE coordinates	L_{max} (cd m^{-2})	EQE$_{max}$ (%)
10	4.1	438	(0.15, 0.04)	2751	3.01
20	3.8	438	(0.15, 0.05)	2726	3.03
30	3.7	438	(0.15, 0.06)	3521	3.11
100	3.3	440	(0.16, 0.08)	5062	3.60

References

1 T. Lu and F. Chen, *J. Comput. Chem.*, 2012, **33**, 580–592.

2 W.-C. Chen, Y. Yuan, Z.-L. Zhu, S.-F. Ni, Z.-Q. Jiang, L.-S. Liao, F.-L. Wong and C.-S. Lee, *Chem. Commun.*, 2018, **54**, 4541–4544.